Journal of Loss Prevention in the Process Industries 79 (2022) 104816

Contents lists available at ScienceDirect

Journal of Loss Prevention in the Process Industries

journal homepage: www.elsevier.com/locate/jlp

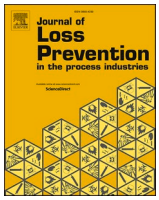

Experimental investigation of a micelle encapsulator F-500 on suppressing lithium ion phosphate batteries fire and rapid cooling

Shuai Yuan, Chongye Chang, Jianqi Zhang, Yifan Liu, Xinming Qian *

State Key Laboratory of Explosion Science and Technology, Beijing Institute of Technology, Beijing, 100081, China

ARTICLE INFO

Keywords:
Lithium-ion battery
Micelle encapsulator
Fire suppression
Thermal runaway

ABSTRACT

Thermal runaway (TR) in lithium-ion batteries (LIBs) and LIB fires have attracted a considerable amount of attention. In this study, the micelle encapsulator F-500 was experimentally investigated to understand its extinguishing effect and cooling capacity for lithium iron phosphate (LFP) cells in modules. The gases produced from the batteries were collected and analysed. The extinguishing effectiveness and cooling capacity of a 3% F-500 solution and pure water mist (WM) were compared and discussed. Furthermore, the concentration of H_2 was evaluated during the tests. The experimental results showed that H_2 is the major gas released during thermal runaway. The combustion of LFP batteries requires external ignition and fire-intensified TR propagation in the LFP battery module. The cooling capacity of the 3% F-500 solution was appropriately three times that of WM according to temperature reduction calculations. The peak concentration for H_2 was 14 ppm when the micelle encapsulator was employed, while the peak concentration was 217 ppm when WM was applied. The control mechanisms were qualitatively discussed by comparing the connection between thermal runaway and fire progress. The cooling effect was identified as the most significant factor not only for rapidly extinguishing LIB flames but also for preventing TR propagation. These results are expected to provide guidelines for fighting LIB fires and for cooling LIB systems.

1. Introduction

Lithium-ion batteries (LIBs) have been widely utilized in the field of fully electric vehicles (EVs) and electrochemical energy storage units due to their high energy density, lack of memory and long lifespan. Nevertheless, LIBs readily experience TR under extreme conditions, such as during overheating (Li et al., 2019), overcharging (Huang et al., 2019), external short circuits (Tao et al., 2020) and acupuncture (Wilke et al., 2017). TR is accompanied by the release of combustible gases, by fires and by even explosive accidents. According to some limited data, in China, the number of EV fire-related accidents reached seventy-six during 2021, as shown in Fig. 1. On 16 April 2021, fire and explosive accidents occurred in an energy storage power station in Beijing, China, which resulted in three people dying and one being injured. Therefore, the control of LIB fires is a technical barrier against promoting the large-scale use of energy storage systems.

LIB failure usually occurs due to short circuiting, which results in a large current in the battery (Yuan et al., 2021). The failure increases the temperature inside the battery. Generally, the main components of the battery include the housing, electrolyte, anode, cathode and separator (Golubkov et al., 2014). As the temperature increases, the electrolyte in the cell housing undergoes vaporisation, which results in an increase in the pressure in the cell. Then, safety venting is observed once the pressure inside exceeds the sum of the fixed pressures of the relief valve crack and the environmental (Chen et al., 2019b). The opening of the safety valve is accompanied by a hissing sound and ejection of flammable liquid (Weng et al., 2019). Therefore, sound is also considered a method of LIB fire detection. As the temperature of the cell increases, large quantities of combustible gases are released from the safety valve. Thermal runaway (TR) occurs in the battery when the integrity of the separator is completely lost, which results in exponential temperature increases (Feng et al., 2014). When the concentration of flammable gases reaches the flammability limits, sparks are released from the safety valve, which can ignite the fuel mixture of the battery (Wang et al., 2019). Additionally, TR is often accompanied by jet flames, heat generation and toxic gas generation. According to reports from most accidents, the TR of individual batteries amplifies the heat level, which often triggers TR in adjacent cells (Gao et al., 2019). This phenomenon is

* Corresponding author.
E-mail address: qsemon@bit.edu.cn (X. Qian).

https://doi.org/10.1016/j.jlp.2022.104816
Received 22 February 2022; Received in revised form 8 April 2022; Accepted 7 June 2022
Available online 17 June 2022

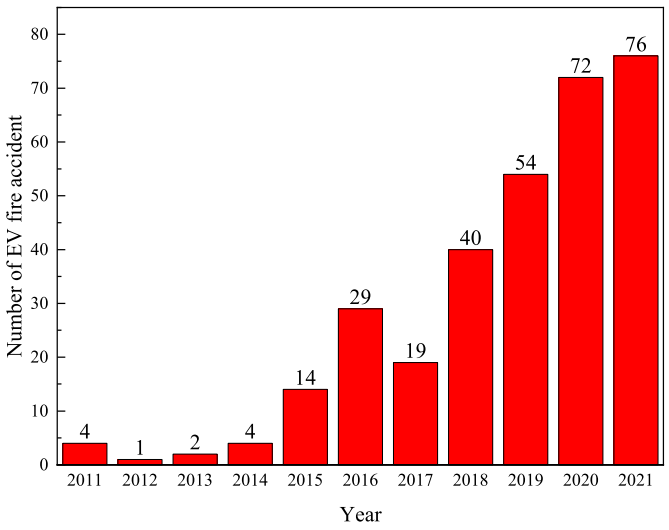

Fig. 1. Summary of EV fire accidents in the past ten years in China.

called thermal propagation.

Researchers have conducted significant experimental investigations on the suppression of single LIB fires. For instance, dry powder can suppress LFP battery fires under appropriate conditions but cannot effectively reduce the temperature of the battery due to its poor cooling capacity (Meng et al., 2020). Heptafluoropropane (HFC-227ea) possesses excellent thermal conductivity (0.016 W/m/K) and can be used as a substitute for Halon. Wang et al. (2016) investigated the inhibition efficiency of the heptafluoropropane (HFC-227ea) extinguishing agent HFC-227ea on lithium titanate (LTO) battery fires. Experimental results indicated that HFC-227ea can extinguish a single battery fire within 25 s. However, the agent must be applied as early as possible to avoid reignition of the battery due to the agent's poor specific capacity (0.94 kJ/kg•°C). However, carbon dioxide (CO_2) is not able to completely suppress LTO battery flames (Wang et al., 2018), and extinguished batteries can reignite after CO_2 is applied due to the low specific capacity (0.85 kJ/kg•°C) and poor thermal conductivity (0.069 W/m/K) of CO_2 (Zhuang et al., 2019). Dodecafluoro-2-methylpentan-3-one ($C_6F_{12}O$) has been widely used in fire prevention applications owing to its excellent cooling capacity. Experimental results showed that the clean agent possessed rapid extinguishing efficiency for $Li(Ni_{1/3}C-o_{1/3}Mn_{1/3})O_2$ (NCM) battery fires (Liu et al., 2018). With the increase in the inhibitor dose of $C_6F_{12}O$, the toxicity of the extinguished combustion system increased. The toxicity index M_{FED1} reached 0.75 when the inhibitor dose was 7.7. However, the peak temperature of the battery was still high due to its nonspecific capacity (1.013 kJ/kg•°C). Some studies have indicated that intermittent spray cooling can improve the cooling capacity of $C_6F_{12}O$ (Meng et al., 2022). Additionally, other auxiliary methods, such as water mist technology, are needed to enhance the cooling capacity (Liu et al., 2020b; Zhang et al., 2020b). However, recent research has shown that the application of $C_6F_{12}O$ increases toxicity problems (Liu et al., 2022). As a clean and effective cooling technology, water mist (WM) was investigated to explore the influence of the critical triggering temperature (Huang et al., 2021; Liu et al., 2019; Xu et al., 2022), different hazard stages (Liu et al., 2021a) and spray durations (Huang et al., 2021; Zhang et al., 2020a) on the WM cooling and control effect on TR. Xu et al. (2020) compared the effectiveness of various fire-extinguishing agents on extinguishing LIB fires. The results indicated that WM possessed a better cooling capacity and suppressed fires more rapidly than CO_2 and HFC-227ea. However, many batteries are assembled with series-parallel connection modules and packs. Therefore, it is important to investigate the effectiveness of fire-extinguishing agents on suppressing TR propagation and battery module fires.

The cooling effect of WM on TR propagation in battery modules has attracted considerable attention in studies. A number of studies have analysed the impact of parallel connections (Liu et al., 2021b), critical temperature (Guo et al., 2021; Liu et al., 2020a; Xu et al., 2022), WM release duration (Xu et al., 2022), and WM working pressure (Guo et al., 2021) on the cooling control effect of WM on TR propagation. Even though water has a high cooling capacity, extinguished batteries can reignite after water flow has ceased (Ditch, 2018). O. Said et al. investigated the effect of WM on TR propagation speeds, and 40% and 50% of battery fires could be effectively prevented when WM was applied at 1.0 and 1.6 g/s, respectively (Said et al., 2021). Compared with WM, $C_6F_{12}O$ exhibited larger reductions in TR propagation and extinguishing efficiency (Said and Stoliarov, 2021). Previous studies indicated that $C_6F_{12}O$ performed the best for extinguishing fires among four fire-extinguishing agents, and WM showed the best cooling capacity and the best ability to control TR propagation (Zhao et al., 2021). However, WM has disadvantages, namely, poor uniformity and difficulty reaching the battery surface (Russo et al., 2018). To reduce water consumption during LIB fire fights, water additives such as F-500 (Egelhaaaf et al., 2013), Firesorb and boron-based liquid fire suppressants (Un and Aydın, 2021) have been employed to suppress LIB module fires. Most previous studies have focused on the cooling effect or extinguishing effectiveness of fire-extinguishing agents. However, related works on the connection between controlling TR propagation and extinguishing LIB fires are rarely considered.

In this study, a micelle encapsulator was investigated to understand its effect on suppressing TR propagation in an LFP battery module and its effect on extinguishing fires. To explore the absorption mechanism of the micelle encapsulator, the gases released from an LFP battery with full charge were collected and analysed. A gas absorption test was conducted to explore the gas encapsulating capacity of the micelle encapsulator. Meanwhile, its absorption capacity was characterized by dynamic laser light scattering (DLS). Comparisons were conducted to evaluated the behaviour of the same array in air (without any additives) and with WM. Finally, relationships between controlling TR and extinguishing fires was discussed.

2. Experiments

2.1. LIB

A single type of cylindrical LIB was chosen as the sample battery in this study. The size of the battery was 32 mm (D) × 141 mm (L). The positive electrode material of the sample battery was $LiFePO_4$. Its nominal voltage and nominal capacity were 3.2 V and 15,000 mAh, respectively. A NEWARE CT-4008T battery testing system connected by a computer was used to prepare the cell sample. Each sample was first discharged to 2 V with a constant current of 5000 mA. Then, the samples were charged to 3.65 V with a constant current of 5000 mA until the current was reduced to 60 mA. Finally, the samples were discharged to the desired state of charge (SOC) with a constant current of 5000 mA. Every battery used in the tests was charged to 100% SOC.

2.2. Experimental process

2.2.1. Characteristic gases in the battery tests

Fig. 2 illustrates a schematic diagram of the experimental setup used for collecting gases produced from the battery sample. The device was a cylindrical tank with an inner diameter of 250 mm and a height of 300 mm. The experimental tank consisted of a gas distribution system, a heating system, and a test system. In addition, the gas distribution system included a helium gas bottle, a vacuum pump and a gas sampling valve. The test system included temperature and overpressure measurement devices.

Before the experiment, the plastic packaging of the sample battery was removed, and the battery was attached to a 500 W electric heater

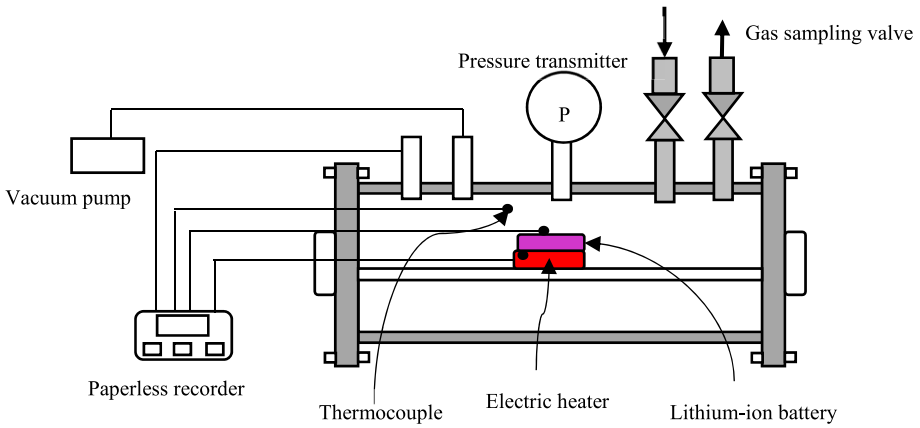

Fig. 2. Schematic diagram for the TR gas collection device.

with nickel chrome wiring. At the beginning of the experiment, the air inside the tank was drawn out by a vacuum pump. A certain amount of helium gas was injected into the tank, which was done three times to ensure that the tank was filled with helium gas. Furthermore, the pressure of the tank was regulated to 1 atm pressure (0.1 First, the heater was heated a rate of 10 °C/min, and the maximum temperature was 300 °C. The heater was turned off once TR was triggered in the tested battery. Finally, the released gases were collected by a high-temperature air collection bag and analysed by gas chromatography and mass spectrometry (GCMS, SHIMADZU GCMS-TQ8040NX). MS was used to detect the TR gases. The GC was calibrated for H_2, CO_2, CO, CH_4 and C_2H_4. The carrier gas was helium. To ensure the reliability of the experiments, the tests were repeated at least once.

2.2.2. *Gas absorption test*

The micelle encapsulator F-500 belongs to a surfactant chemical family based on its current material safety data sheet (MSDS). This material consists of an aqueous mixture whose quantitative composition is unavailable, and the exact concentrations of components are considered a trade secret. Its components include 40%–50% fatty alkyl ether reaction products with aliphatic acids, 5%–8% alcohols and 2%–4% 2,2′,2″-nitrilotrisethanol aliphatic acid soap. However, the precise molecular formula and molecular structure of F-500 are unavailable because it is a trade secret. To understand the absorption capacity of the 3% F-500 solution for H_2, a preparation device for standard gas samples was established to carry out gas absorption tests, as shown in Fig. 3. First, the characteristic gases released from battery TR were injected into a 1000 ml conical flask filled with fresh 3% F-500 solution. Each test was operated for 30 min to prepare a gas-saturated solution. Finally, the micelle size of the gas-saturated solution was measured by a laser particle size analyser (Malvern 3000).

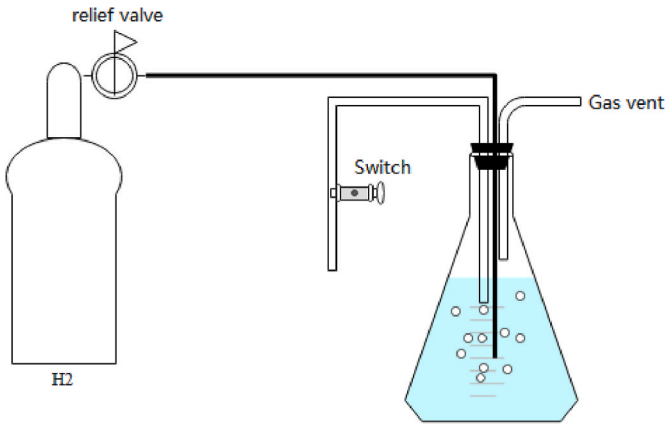

Fig. 3. Schematic diagram of the gas absorption device.

2.2.3. *Fire extinguishing test*

A schematic diagram of the fire-extinguishing test apparatus is shown in Fig. 4. The apparatus was a cuboid of dimensions 0.7 m × 1.015 m × 1.82 m. The apparatus mainly included a combustion chamber, a high-pressure water spray system, an exhaust system, a heating system, a sampling system, a thermocouple data logger and a digital video camera. The entire experiment was recorded by a digital video camera at 50 fps. The sample gases were passed through a ring sampler and then filtrated and dried. Finally, the hydrogen concentration was detected by a gas analysis device with a range of 0–12,000 ppm. The gas concentration data was obtained by gas analysis at 5 s time intervals. The high-pressure water spray system was composed of five main subsystems, including a tank, pressure gage, fire-extinguishing pipe, solenoid valve and nozzle.

In this study, a 500 W electric heater with the same size battery sample was placed next to the other three batteries to simulate an actual scenario for a battery module, as shown in Fig. 5(a). The heater and batteries were bundled with nickel chrome wire and clamped with two stainless steel holders to fix the geometry of the battery module and prevent the batteries from escaping, as shown in Fig. 5(b). Furthermore, the heater was used to trigger TR in the battery. Based on previous research, an external fire source was necessary to ignite the combustible gases (Zhang et al., 2020c). Therefore, an external electric spark was used to ignite the combustible gas and electrolyte vapours. A spark is produced when a voltage of 20 kV breaks through the air. The spark was generated in the upper middle portion of the battery module. The distance between the external electric spark and the upper part of the battery module was approximately 10 cm. Three K-type (T2-T4) thermocouples were employed to measure the temperatures of the batteries. The other two K-type (T5-T6) thermocouples were located at 20 cm and 38 cm above the upper middle position of the battery module. T5-T6 thermocouples were used to measure the flame temperatures, as shown in Fig. 5(b). Moreover, one K-type (T1) thermocouple was used to monitor the temperature of the heater and control its temperature increase. Its temperature increase and maximum temperature were the same as the conditions in Section 2.2.1. The distance between the nozzle and the battery was approximately 46 cm, and the spray angle of the agent was 60° to ensure the water mist could completely cover the LIB fire. The flow discharge coefficient of the nozzle was 0.22 L min^{-1} $MPa^{-0.5}$. The pressure of the WM system was fixed at 5.5 MPa, and the flow rate of the nozzle was 1.62 L/min. The flow discharge coefficient can be determined by Equation (1):

$$Q = K\sqrt{10P} \tag{1}$$

where K is the flow discharge coefficient. The related parameters for the

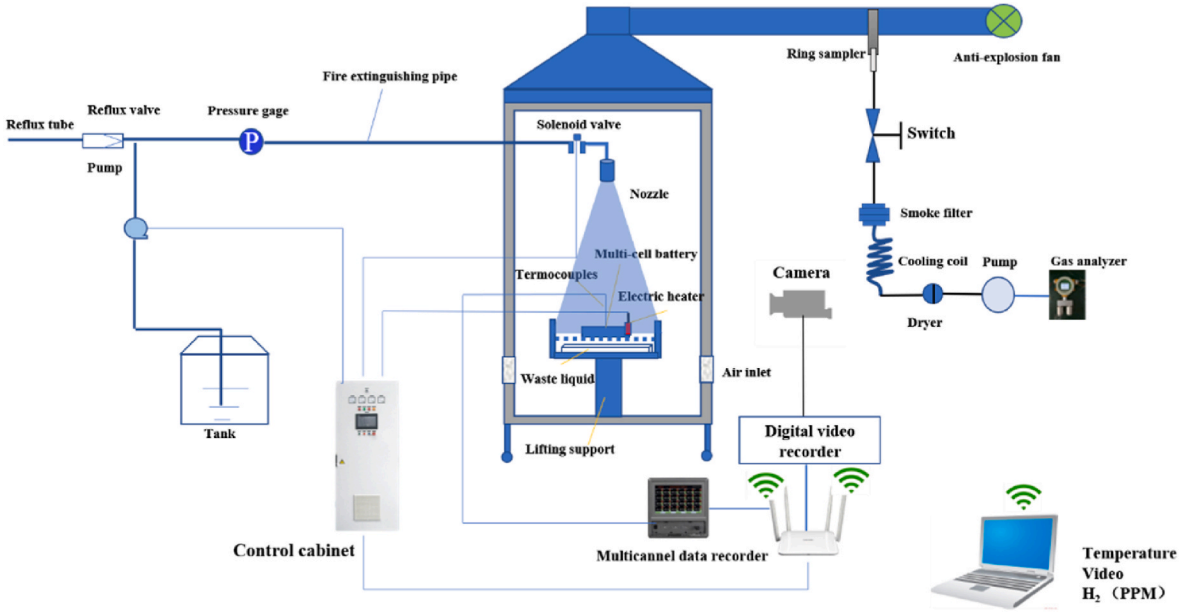

Fig. 4. Schematic of the experimental apparatus for LIB TR suppression.

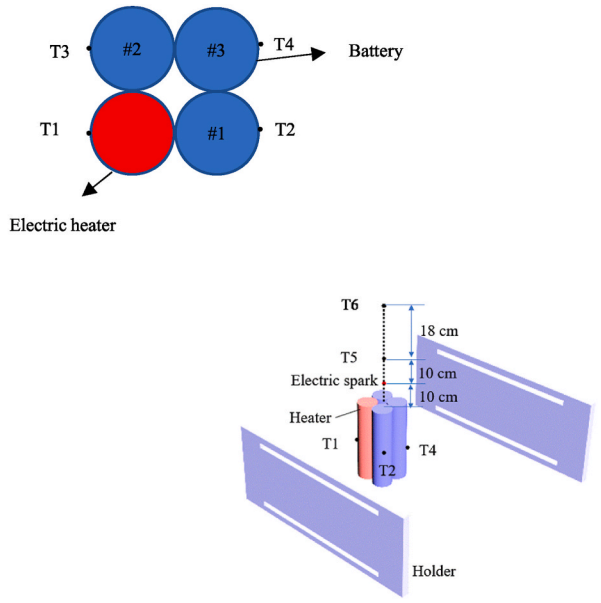

Fig. 5. (a) Distribution of the tested battery modules. (b) Arrangement of the thermocouples and electric spark.

agent and WM are listed in Table 1.

Table 2 lists the experimental conditions for the LIB fire suppression tests. For test 1, a combustion test was conducted to understand the combustion behaviour of the LFP battery module. The fire extinguishing efficiency of a 3% F-500 solution was compared with WM as the benchmark in test 2. Fig. 6 indicates the experimental procedure. An electric spark was triggered to ignite the combustible gases when the safety valve of the battery was open. Then, the electric spark generator was turned off until a jet fire was observed. The surface temperature of the batteries reached 250 °C, and then the heater was turned off. Based on our previous tests, the surface temperature of the battery was over 300 °C, which was considered the TR temperature of the battery. Hence, the fire-extinguishing agent was applied when the temperature of the first battery was above 300 °C. The duration time was fixed to 30 s for all the extinguishing tests conducted in this study. To obtain reliable data, each test was repeated at least two times.

Table 1
Characteristics of the agent.

Agent	Nozzle working pressure (MPa)	Flow discharge coefficient ($Lmin^{-1}MPa^{-0.5}$)	Flow rate (L/min)	Mass of agents
WM	5.5	0.22	1.62	0.81
3% F-500	5.5	0.22	1.62	0.81

Table 2
Experimental conditions for the tests.

No.	SOC/ %	Agents	Pressure/ MPa	Duration/ s	Release time
1	100	/	/	/	/
2	100	WM	5.5	30	Above 300 °C
3	100	3% F-500 solution	5.5	30	Above 300 °C

3. Results and discussion

3.1. Temperature variations in the battery module without the 3% F-500 solution

To understand the combustion behaviour of the LFP battery module, the surface temperature of the battery and the flame temperature without additives were investigated, as illustrated in Fig. 7. The two inserted pictures indicate experimental smoke venting and combustion behaviours. A large amount of smoke was produced at 2160 s due to smoke venting, and the temperature of the cell was appropriately 100 °C at that time, which did not satisfy combustion conditions. Therefore, a high voltage pulse igniter was used to ignite the combustible gases and flammable liquids. This procedure is consistent with the results of previous studies (Liu et al., 2022). However, the smoke was not immediately ignited by the igniter, which may be because the smoke gases did not reach their combustion threshold. The delay in the ignition time may have influenced the TR reaction and the temperature of the battery.

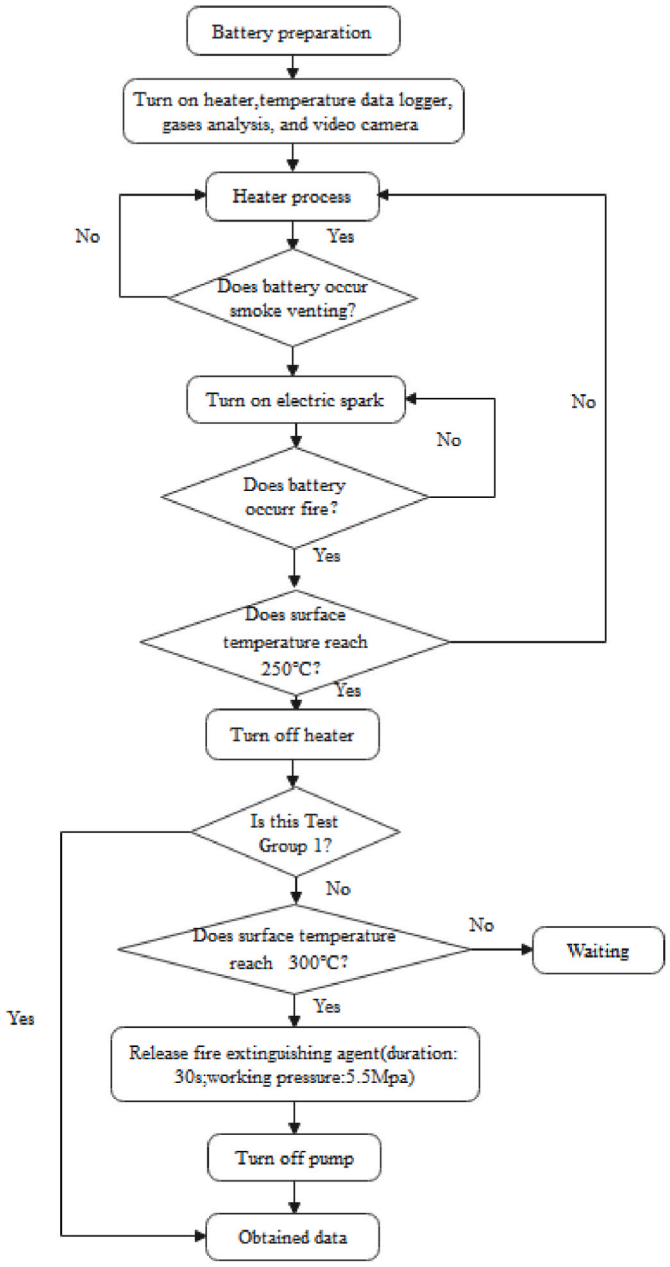

Fig. 6. Flowchart of the test procedure.

Future work should therefore include a delay in ignition to evaluate the influence of the delay on the TR reaction process and the temperature of the battery. The gases were ignited 306 s after the safety valve was opened. The flame was maintained for approximately 499 s in this test. Previous results have indicated that LCO and $Li(Ni_xCo_yMn_z)O_2$ cells tend to release more mars, which form the main heat source for combustion (Chen et al., 2019a; Liu et al., 2020a). However, these mars were not observed in our work. This finding is very valuable for evaluating the battery module fire risk grade. When the thermocouple of any of the batteries reached 250 °C, the heater was turned off. Then, TR propagation relied on heat transfer from neighbourhood batteries. TR occurs when temperature increases at an exponential rate. Hence, the TR onset temperature (T_r) of a battery is a significant parameter. In our study, T_r was chosen to be the critical temperature at which the rate of temperature increase reached 10 °C/s. As shown in Fig. 7(b), TR first occurred in battery #1 when the surface temperature of battery #1 reached 139.9 °C. The considerable amount of the heat produced by TR was transferred to two other cells, which resulted in TR propagation. The maximum temperature of battery #1 reached 283.7 °C, while those of battery #3 and battery #2 were 520.4 °C and 401.6 °C, respectively.

Fig. 8 illustrates the surface temperature response of the batteries and the temperature response of the flame in test 2. The temperature variation in battery #1 was similar to that of battery #2 due to their symmetrical arrangement. WM was discharged when the temperature of any cell reached 300 °C. The surface temperature of battery #2 reached 300 °C first in test 2. As shown in Fig. 8(b), the temperature of battery #2 rapidly increased initially and then decreased during WM application. The heat dissipation of battery #2 mainly relied on the sum of the vaporisation latent heat and specific heat of water, which can be calculated with Equation (2). To precisely measure the $\dot{q}_w$, we put a 500 ml beaker under the nozzle to measure the volume of water in a certain area before the experiment. The volume of water reached 10 ml in 10 s. Based on the relationship between the area of the 500 ml breaker and the battery module, $\dot{q}_w$ could then be calculated from the result.

$$p_w = \begin{cases} c_w \rho_w \bullet q_w (T - T_0); & T < T_{boil} \\ c_w \rho_w \bullet q_w (T_{boil} - T_0) + h_f \rho_w \bullet q_w; T \geq T_{boil} \end{cases} \quad (2)$$

where p_w is the cooling power, c_w is the specific heat of water (4.12 kJ/kg•°C) and ρ_w represents the density of water (1000 kg/m^3). $\dot{q}_w$ is the volume flow rate of WM on individual batteries (2.85×10^{-7} m^3/s), and T_0 indicates the ambient temperature (20 °C). T_{boil} represents the boiling temperature of water (100 °C) and h_f stands for the vaporisation latent heat of water (2257 kJ/kg). Therefore, the cooling power p_w was 737.1 W.

The heating power of the cell can be expressed by the following equation:

$$p_H = m_b c_b \dot{T} \quad (3)$$

where m_b is the mass of the battery after the test, c_b represents the specific heat of the cell (1.072 kJ/kg•°C) and $\dot{T}$ is the rate of increase of temperature. Fig. 9 illustrates the p_H change of the batteries in test 1. The p_H was 6377 W when the temperature of the first battery reached 300 °C.

Clearly, the heating power was higher than p_w (737.1 W). However, the battery heat power was reduced to 0 W in 7 s due to momentary TR. Therefore, the surface temperature of battery #2 rapidly increased initially and then decreased during WM application. The significant parameters from test 2 are listed in Table 2. According to the battery maximum temperatures, WM showed good cooling performance. For instance, the maximum temperature (T_{max}) of battery #1 was decreased from 283.7 °C to 217 °C by WM, as shown in Table 3. The maximum temperature of battery #2 was decreased from 401.6 °C to 372.3 °C, as shown in Table 2. The peak temperature of battery #3 was decreased from 520.4 °C to 128.4 °C by the WM. The temperatures of battery #1 and battery #2 initially decreased and then rebounded to 169.3 °C and 255.8 °C after the application of WM, respectively. This is because the water dried up, and the internal temperatures of the batteries were still high (Zhang et al., 2022). However, the surface temperature of battery #3 did not vary considerably, and it retained a low temperature (approximately 102.5 °C). Therefore, reducing the temperature (T_R) of a battery experiencing TR to below 102.5 °C is essential for preventing temperature rebound. Additionally, the cooling rate when the WM spray was ceased (approximately 30 s), defined as dT_1/dt_1, was different for the different batteries due to their different cell temperatures when the water mist was applied (T_w). For example, the surface temperature of battery #1 was 204.9 °C when water mist was released, while the surface temperatures of battery #2 and battery #3 were 320.9 °C and 123.3 °C, respectively. The cooling rate when the temperature of the battery reached the reduced temperature, defined as dT_2/dt_2, represents the comprehensive cooling ability. Understandably, the cooling rate of water increases with the increasing surface temperature of the battery.

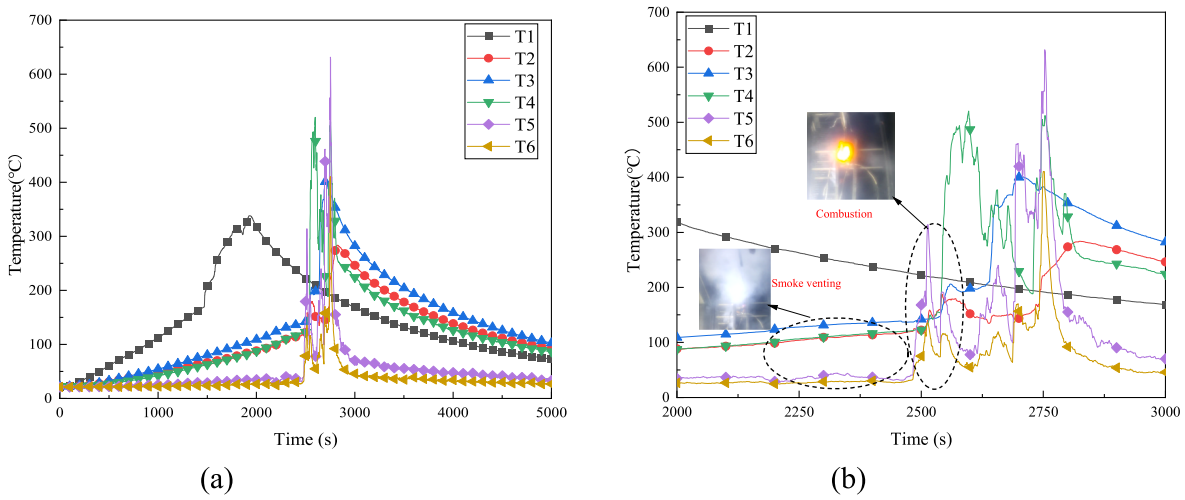

Fig. 7. Temperature of the battery and flame in case 1 (a), and (b) is a partial enlargement of the 2000–3000 s region.

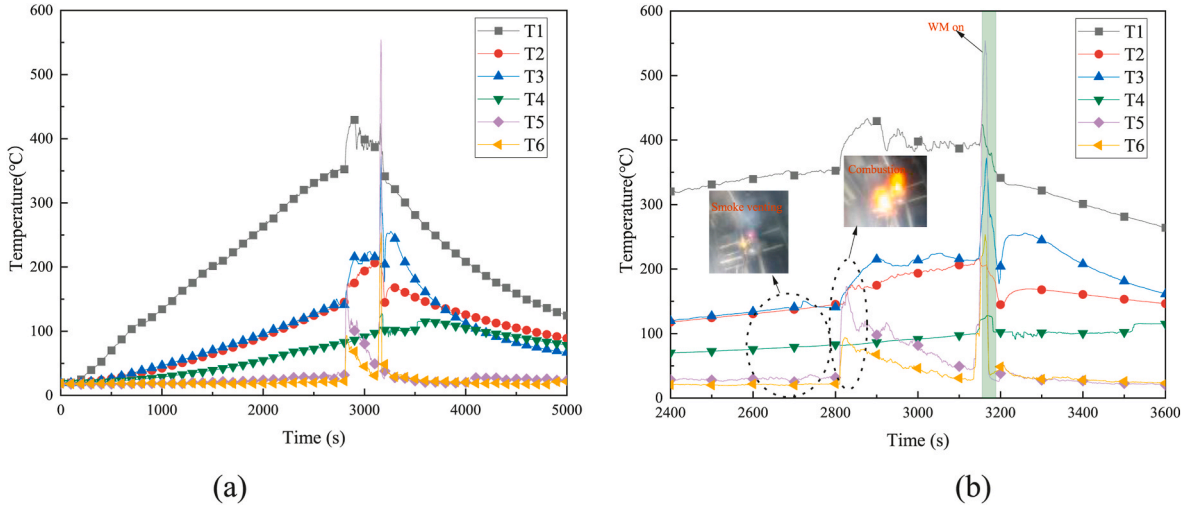

Fig. 8. Temperature of the battery and flame in case 2 (a), and (b) is a partial enlargement of the 2400–3600 s region.

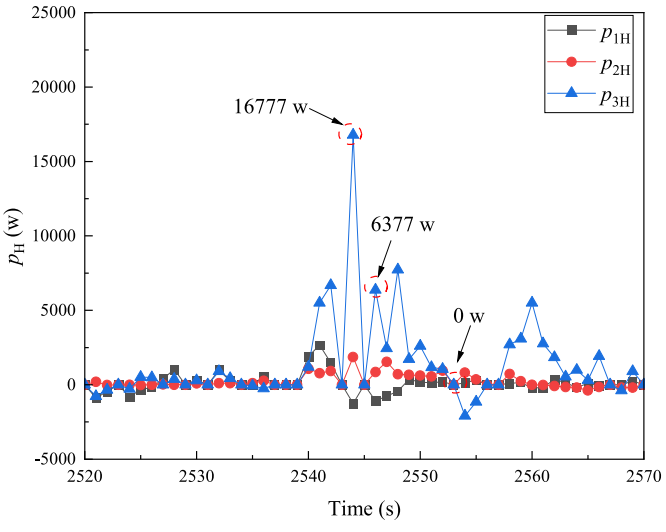

Fig. 9. p_H change of batteries in test 1.

Table 3
Key parameters of the batteries in test 2.

Item	#1	#2	#3
T_{max} (°C)	217	372.3	128.4
T_w (°C)	204.9	320.1	123.3
T_R (°C)	169.3	255.8	102.7
dT_1/dt_1 (°C/s)	−1.06	−3.34	−0.70
dT_2/dt_2 (°C/s)	−0.36	−0.64	−0.34

3.2. *Cooling effect of a 3% F-500 solution on a battery module*

The surface temperature curves for the battery and flame temperatures of the battery module with a 3% F-500 solution are shown in Fig. 10. The 3% F-500 solution was discharged immediately when the temperature of battery #1 reached 300 °C. The temperatures of the cells show a slight increase and then decrease. According to the battery maximum temperatures, the 3% F-500 solution exhibited excellent cooling performance. For instance, the maximum temperature of battery #2 decreased from 401.6 °C to 154.6 °C, as shown in Table 2. The maximum temperature of battery #3 was decreased from 520.4 °C to 327.7 °C by 3% F-500 solution. Additionally, the rebound temperatures of the cells were maintained at approximately 100 °C, which were lower

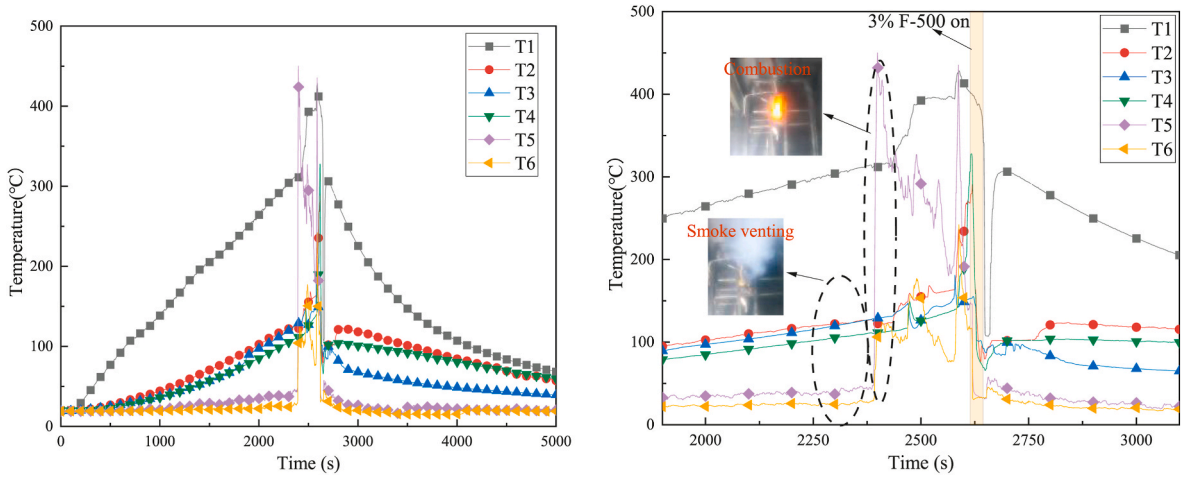

Fig. 10. The temperature of the battery and flame in case 3 (a), and (b) is a partial enlargement of the 1900–3100 s region.

than those of the batteries when WM was applied. Meanwhile, the cooling rates of the cells when 3% F-500 was applied were higher than those of the cells when WM was applied, as shown in Table 4. One of the main goals of this experiment was to attempt to find a way to quantify the cooling capacity of a water-based fire-extinguishing agent for a battery module. A quantitative parameter is significant for evaluating the cooling effectiveness of agents. In this study, the quantitative average temperature, T_d, was calculated by Equation (3) (Maloney and Administration, 2017). The calculation of T_d was achieved by using the average initial temperatures of the three batteries and electric heater and subtracting the average temperature of the battery module for 100 s.

Fig. 11 shows a plot of the calculated average T_d for different tests. The cooling capacity of the 3% F-500 solution was three times higher than that of WM based on T_d, as shown in Fig. 11. Our results provide compelling evidence for quantification of the cooling capacity of fire-extinguishing agents for battery modules. Based on our previous research results, F-500 reduces the surface tension of pure water from 69 to 23 mN/m, which allows for the formation of smaller water droplets and expands the specific surface area of the water droplets. In addition, lower surface tension enhances the permeability of water such that it can enter the gaps in the battery module, which speeds up the endothermic reaction of water. The unique molecular structure of F-500 is also significant for rapid cooling. The nonpolar side of the F-500 molecule orients away from the water droplets. The heat from the LIB fire converts the nonpolar side to a polar side in the F-500 molecule. Hence, the heat is absorbed by water, dissolving the polar side of F-500, as shown in Fig. 12. In contrast with the heat absorption of pure water to convert to steam, the 3% F-500 solution absorbs the heat content by thermal conveyance. Therefore, F-500 reduces the evaporation of water and improves the cooling efficiency of water.

$$T_d = \frac{\sum_{i=1}^{5} T_{i,time=0}}{5} - \frac{\sum_{j=1}^{100}\sum_{i=1}^{5} T_{i,j}}{500} \quad (4)$$

Table 4
Key parameters of the batteries in test 3.

Item	#1	#2	#3
T_{max} (°C)	290.8	154.6	327.7
T_F (°C)	268.2	152.6	306.1
T_R (°C)	101.9	96.8	103.9
dT_1/dt_1 (°C/s)	−5.87	−1.95	−7.84
dT_2/dt_2 (°C/s)	−2.87	−1.03	−1.10

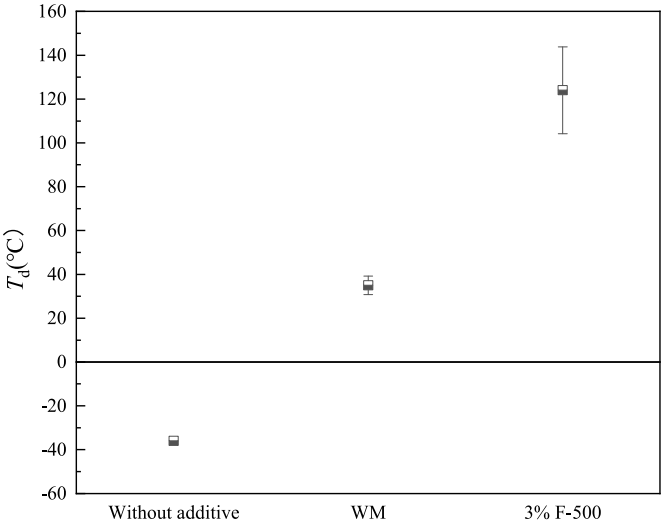

Fig. 11. Temperature drop, T_d, for various fire-extinguishing agents.

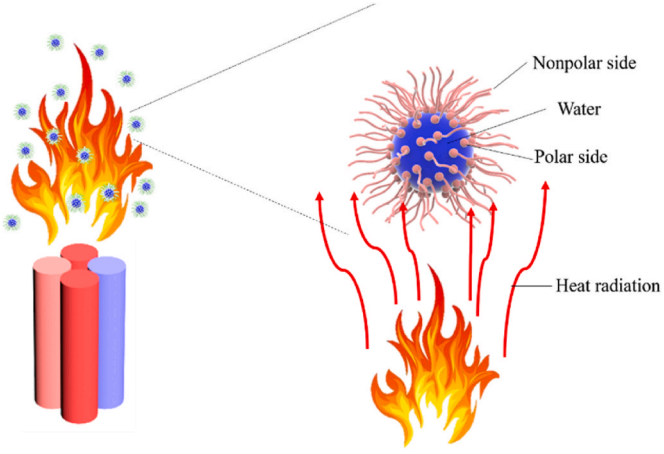

Fig. 12. Cooling mechanisms of F-500 on battery module fires.

3.3. Effect of a 3% F-500 solution on gas concentration

As mentioned above, a large amount of gas was released from the safety valves of the batteries. Hence, detecting the components and

percentages of gases is necessary to understand the combustion behaviour of LIBs. Data obtained in previous studies indicated that H_2 and CO_2 were the major gases (Golubkov et al., 2014). In our study, H_2, CO_2, CH_4, CO and C_2H_4 were measured, as illustrated in Fig. 13. The highest proportion of components were H_2 and CO_2, which is consistent with results obtained in previous studies. H_2 accounted for 30.9% in previous studies (Golubkov et al., 2014), while H_2 accounted for 69.79% of the gases released in our work. According to Golubkov et al. (2015), the amount of H_2 increases with increasing SOC in LFP batteries. The capacity of the 32141-type battery used in this work was higher than that of the 18650-type battery used in previous studies (Golubkov et al., 2014). This is why the battery used in this work produced a larger amount of H_2. Hence, H_2 was chosen as the characteristic gas for the LFP battery in this work due to its flammability and explosivity. H_2 was released from chemical reactions between binder materials (PVDF or carboxymethyl cellulose) (Du Pasquier et al., 1998; Wang et al., 2011):

$$\text{-}CH_2\text{-}CF_2\text{-} + Li \rightarrow LiF + \text{–}CH{=}CF\text{-} + 1/2\ H_2 \quad (5)$$

$$CMC\text{-}OH + Li \rightarrow CMC\text{-}OLi + 1/2\ H_2 \quad (6)$$

To explore the influence of the fire-extinguishing agent on the gas concentration, the concentration of hydrogen gas was monitored in all tests, as shown in Fig. 14. The peak concentrations of hydrogen were 476, 217, and 14 ppm in tests 1 through 3, respectively. First, the electrolyte vapour was vented from the safety valve as the temperature gradually increased. Then, a more violent chemical reaction occurred in the battery under the action the external heater. A certain amount of gas was released from the safety valve, and TR occurred inside the battery at the same time.

The maximum concentration of hydrogen decreased regardless of whether WM or the 3% F-500 solution was applied in our study, as shown in Fig. 14. However, a previous study found that batteries produced more H_2 when WM is used (Lin et al., 2020). The results of the previous study suggested that the fire was quickly suppressed when WM was applied, which resulted in the incomplete combustion of the combustible gases. Extinguishing time may be the main factor affecting the concentration of hydrogen gas. Our results confirmed the hypothesis

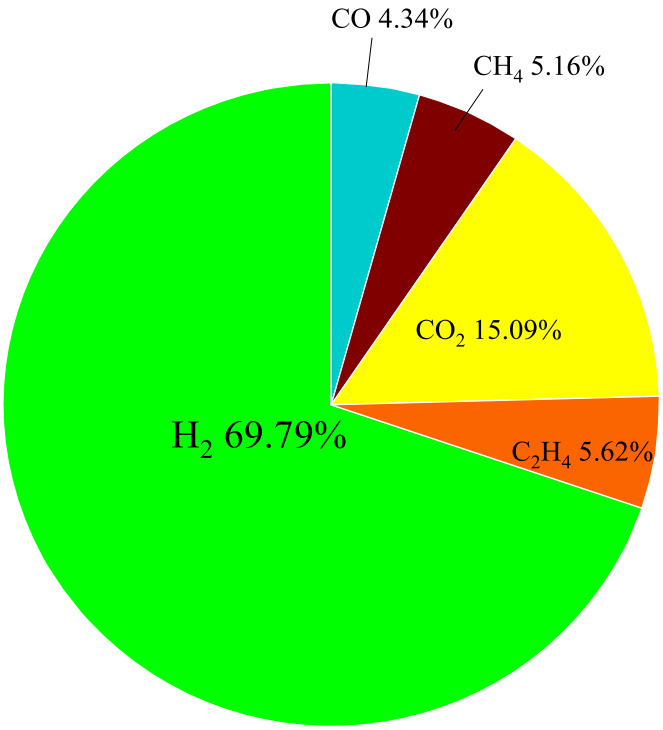

Fig. 13. Detected components of the released gases (vol%).

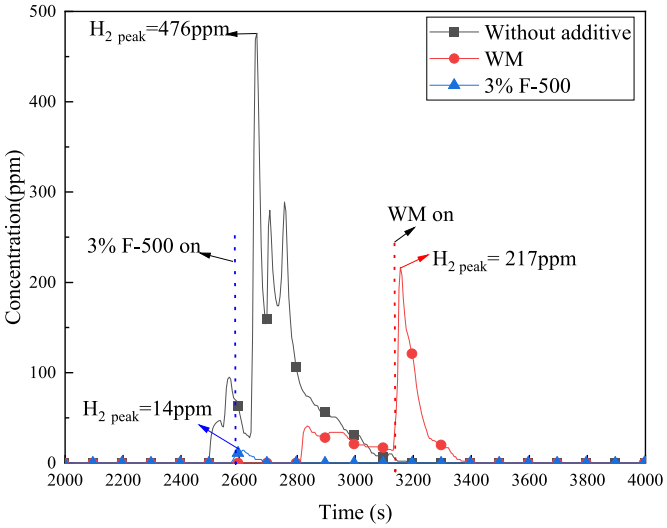

Fig. 14. The concentration responses of hydrogen gas in all tests.

that the maximum concentration of hydrogen is reduced when the fire is not completely inhibited during the application of WM. As discussed above, the 3% F-500 solution possessed a higher cooling efficiency than pure water, which strongly inhibited the chemical reaction within the cell. Therefore, the concentration of hydrogen gas was lower when the 3% F-500 solution was applied than that when WM was applied. To understand the absorption capacity of the 3% F-500 solution for H_2, the micelle size of 3% F-500 was tested before and after the absorption tests. The median particle diameter (D50) for the 3% F-500 solution was 38.15 nm before the absorption tests and 49.76 nm after the absorption of H_2, as shown in Fig. 15. Clearly, the particle diameter of the 3% F-500 solution after the absorption test was larger.

This study therefore indicated that the 3% F-500 solution absorbs H_2. H_2 is a nonpolar gas. Therefore, H_2 is easily captured by the nonpolar side of F-500. As a result, H_2 is solubilized in the interior of the micelle, as illustrated in Fig. 16. The process is spontaneously completed due to a decrease in the Gibbs free energy (Matheson and King, 1978). Most notably, this is the first study to our knowledge to investigate the effectiveness of F-500 for absorbing the characteristic gases produced during LIB combustion. Our results provide compelling evidence for the absorbing functions of a 3% F-500 solution on the characteristic gases produced by LIBs. Nevertheless, some limitations are worth noting. Although our hypotheses were supported, the investigation into the absorption efficiency of the 3% F-500 solution was not thorough. Future work should therefore include encapsulation efficiency work designed to evaluate whether the absorption efficiency of a 3% F-500 solution is retained over the long term in explosion suppression experiments.

3.4. Suppression effect of a 3% F-500 solution on combustion and TR propagation

The extinguishing time and number of TR propagation events are significant parameters in evaluating the effectiveness of fire-extinguishing agents. The extinguishing time in the three tests and the corresponding number of TR occurring in the batteries are shown in Fig. 17. The LIB fire continued for 479 ± 25 s without any additives, and all the batteries in the battery module experienced TR. A large amount of material was ejected from the negative electrode in test 1, as presented in Fig. 18(a). However, the fire was not completely inhibited by WM, and all cells experienced TR in test 2, as shown in Fig. 18(b). The results indicated that WM only controlled the fire, but it could not prevent the other batteries from undergoing TR. The fire was terminated within approximately 13 s in test 3. Furthermore, only one battery experienced TR in test 3, as shown in Fig. 17. The integrity of the battery module in

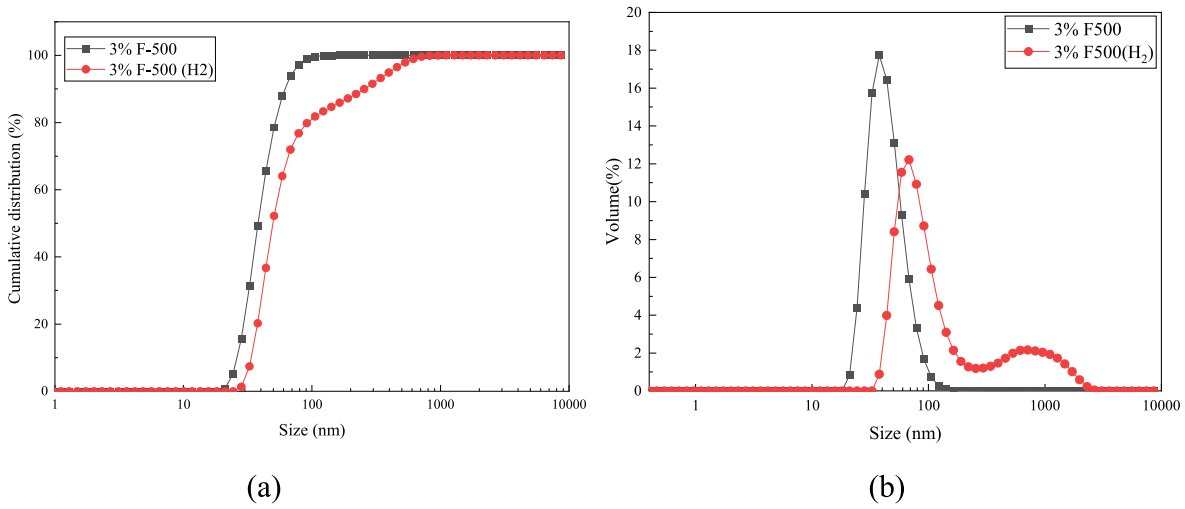

Fig. 15. Micelle size of the 3% F-500 solution before and after absorption tests. (a) Cumulative distribution curve of micelle size; (b) volume distribution curve of micelle size.

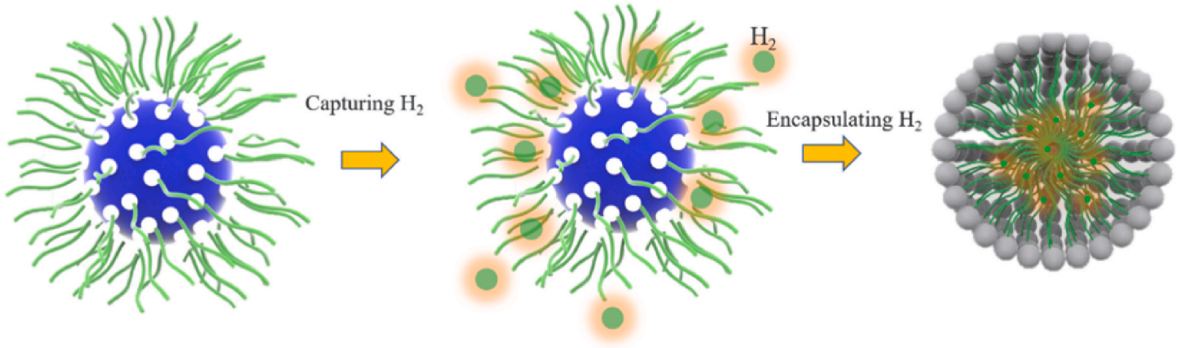

Fig. 16. The micelle formation for hydrogen absorption.

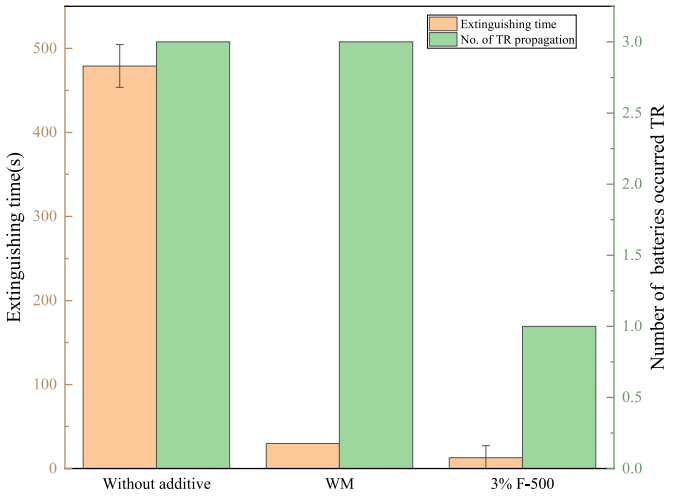

Fig. 17. Extinguishing time and the number of TR occurring in batteries.

test 3 was markedly better than that in test 2, as shown in Fig. 18(c). Compared with WM, the 3% F-500 solution had a more rapid and effective extinguishing effect due to its cooling capacity and ability to absorb hydrogen gas. TR could occur in a battery without an oxidant. Hence, fuel, heat and free radicals are common components of an LIB fire and TR, as illustrated in Fig. 19. A high-efficiency cooling effect is an effective way to reduce oxygen concentration and fuel concentration. Hence, an effective coolant will providing cooling through multiple routes to inhibit fires and prevent TR. Clearly, the two advantages of F-500 are helpful in extinguishing fires. This is why preventing TR propagation in the battery module is conducive to the rapid extinguishing of fires.

4. Conclusions

In this study, the cooling effect and ability of a 3% F-500 solution to extinguish fires in battery modules were investigated through experiments. To comprehensively understand how the fuel in the battery overwent TR, we collected and analysed the components released from the battery. To evaluate the cooling effect and the reduction in key gas concentrations upon the application of the 3% F-500 solution, free-burn tests and pure WM tests were conducted to provide benchmarks. The cooling effects of the fire-extinguishing agents were quantitatively analysed based on the temperature drop they produced. Hydrogen concentration was monitored to explore the absorption mechanism of the 3% F-500 solution. Finally, the relationship between extinguishing efficiency and suppression of TR propagation was analysed. The following points were obtained from this study:

(a) The WM cooling mechanism involves a combination of favourable specific heat and vaporisation latent heat characteristics when the temperature of the battery is higher than the boiling

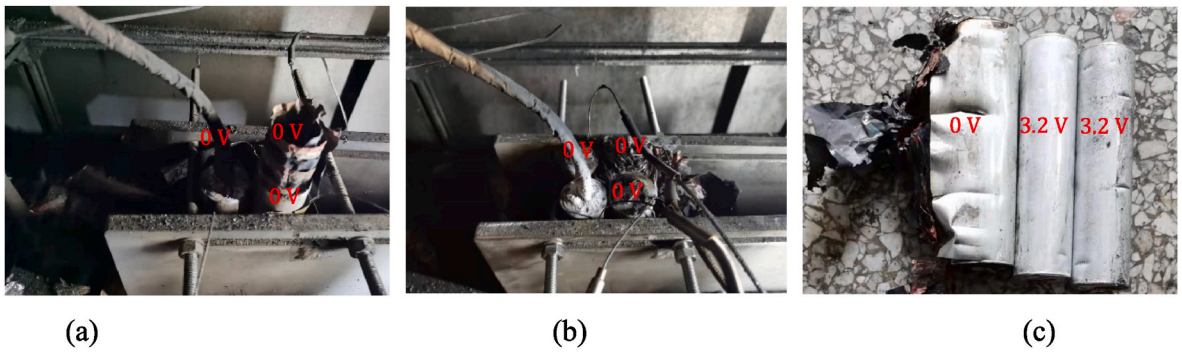

Fig. 18. Battery modules after tests. (a) test 1; (b) test 2; (c) test 3.

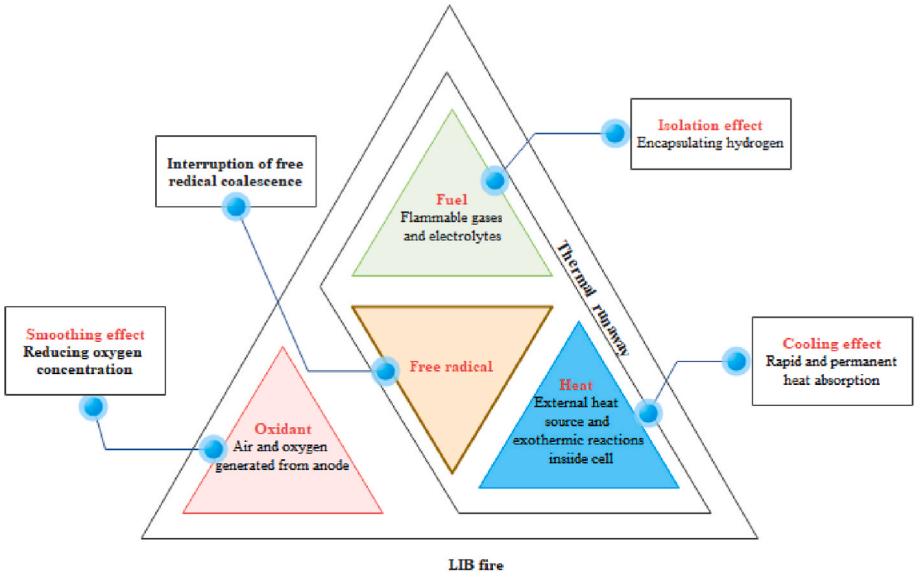

Fig. 19. Suppressing mechanisms of F-500 in the LIB module fire and in TR.

point of water. The cooling rate of water increases with the increasing surface temperature of the battery.

(b) The cooling capacity of the 3% F-500 solution is up to three times that of a WM. The cooling rate of water increases with the increasing surface temperature of the battery. Lower surface tension enhances the permeability of water for entering the gaps in the battery module, which accelerates the endothermic reaction of water. Additionally, the heat from the LIB fire transfers from the nonpolar side to the polar side of F-500 due to its micelle structure.

(c) The 3% F-500 solution reduces the hydrogen concentration when the battery module experiences TR. F-500 absorbs H_2 through its nonpolar side. In contrast, the concentration of hydrogen gas first increases and then decreases when WM is applied.

(d) Stopping TR propagation is conducive to rapidly extinguishing LIB fires. The isolation effect and cooling effect are effective factors in extinguishing fires and suppressing TR. The cooling effect plays the most significant role in extinguishing battery module fires and preventing TR propagation within the battery module.

Author contributions

Shuai Yuan: Conceptualization, Validation, Investigation, Writing-original draft. Chongye Chang: Conceptualization, Methodology, Project administration, Supervision. Jianqi Zhang: Investigation. Yifan Liu: Investigation Xinming Qian: Validation.

Declaration of competing interest

The authors declare that they have no known competing financial interests or personal relationships that could have appeared to influence the work reported in this paper.

Acknowledge

This work was supported by the National Key Research and Development Program of China (grant number 2017YFC0804700).

References

Maloney, T., Administration, U.S.D. of T.F.A., 2017. Extinguishment of Lithium-Ion and Lithium-Metal Battery Fires.

Chen, M., Dongxu, O., Liu, J., Wang, J., 2019a. Investigation on thermal and fire propagation behaviors of multiple lithium-ion batteries within the package. Appl. Therm. Eng. 157, 113750 https://doi.org/10.1016/j.applthermaleng.2019.113750.

Chen, M., Ouyang, D., Weng, J., Liu, J., Wang, J., 2019b. Environmental pressure effects on thermal runaway and fire behaviors of lithium-ion battery with different cathodes and state of charge. Process Saf. Environ. Protect. 130, 250–256. https://doi.org/10.1016/j.psep.2019.08.023.

Ditch, B., 2018. The impact of thermal runaway on sprinkler protection recommendations for warehouse storage of cartoned lithium-ion batteries. Fire Technol. 54, 359–377. https://doi.org/10.1007/s10694-017-0687-6.

Du Pasquier, A., Disma, F., Bowmer, T., Gozdz, A.S., Amatucci, G., Tarascon, J.M., 1998. Erratum: "differential scanning calorimetry study of the reactivity of carbon anodes

in plastic Li-ion batteries" [J. Electrochem. Soc., 145, 472 (1998)]. J. Electrochem. Soc. 145, 1413. https://doi.org/10.1149/1.1838474, 1413.
Egelhaaaf, M., Kress, D., Wolpert, D., Lange, T., 2013. Fire fighting of Li-Ion traction battery. SAE Int. J. Alt. Powertrans. 2, 37–48.
Feng, X., Fang, M., He, X., Ouyang, M., Lu, L., Wang, H., Zhang, M., 2014. Thermal runaway features of large format prismatic lithium ion battery using extended volume accelerating rate calorimetry. J. Power Sources 255, 294–301. https://doi.org/10.1016/j.jpowsour.2014.01.005.
Gao, S., Feng, X., Lu, L., Kamyab, N., Du, J., Coman, P., White, R.E., Ouyang, M., 2019. An experimental and analytical study of thermal runaway propagation in a large format lithium ion battery module with NCM pouch-cells in parallel. Int. J. Heat Mass Tran. 135, 93–103. https://doi.org/10.1016/j.ijheatmasstransfer.2019.01.125.
Golubkov, A.W., Fuchs, D., Wagner, J., Wiltsche, H., Stangl, C., Fauler, G., Voitic, G., Thaler, A., Hacker, V., 2014. Thermal-runaway experiments on consumer Li-ion batteries with metal-oxide and olivin-type cathodes. RSC Adv. 4, 3633–3642. https://doi.org/10.1039/c3ra45748f.
Golubkov, A.W., Scheikl, S., Planteu, R., Voitic, G., Wiltsche, H., Stangl, C., Fauler, G., Thaler, A., Hacker, V., 2015. Thermal runaway of commercial 18650 Li-ion batteries with LFP and NCA cathodes - impact of state of charge and overcharge. RSC Adv. 5, 57171–57186. https://doi.org/10.1039/c5ra05897j.
Guo, J., Wang, H., He, Y., 2021. Inhibition effect of thermally-induced fire in 21,700 lithium-ion battery with low-pressure twin-fluid water mist. J. Electrochem. Energy Convers. Storage 18, 1–7. https://doi.org/10.1115/1.4049569.
Huang, L., Zhang, Z., Wang, Z., Zhang, L., Zhu, X., Dorrell, D.D., 2019. Thermal runaway behavior during overcharge for large-format Lithium-ion batteries with different packaging patterns. J. Energy Storage 25, 100811. https://doi.org/10.1016/j.est.2019.100811.
Huang, Y., Wu, Y., Liu, B., 2021. Experimental investigation into the use of emergency spray on suppression of battery thermal runaway. J. Energy Storage 38, 102546. https://doi.org/10.1016/j.est.2021.102546.
Li, H., Chen, H., Zhong, G., Wang, Y., Wang, Q., 2019. Experimental study on thermal runaway risk of 18650 lithium ion battery under side-heating condition. J. Loss Prev. Process. Ind. 61, 122–129. https://doi.org/10.1016/j.jlp.2019.06.012.
Lin, Z., Qiangling, D., Yujun, L., Jiajia, X., Jinhua, S., Huahua, X., 2020. Experimental investigation of water spray on suppressing lithium-ion battery fires. Fire Saf. J. 103117 https://doi.org/10.1016/j.firesaf.2020.103117.
Liu, Y., Duan, Q., Xu, J., Chen, H., Lu, W., Wang, Q., 2018. Experimental study on the efficiency of dodecafluoro-2-methylpentan-3-one on suppressing lithium-ion battery fires. RSC Adv. 8, 42223–42232. https://doi.org/10.1039/c8ra08908f.
Liu, T., Liu, Y., Wang, X., Kong, X., Li, G., 2019. Cooling control of thermally-induced thermal runaway in 18,650 lithium ion battery with water mist. Energy Convers. Manag. 199, 111969 https://doi.org/10.1016/j.enconman.2019.111969.
Liu, T., Tao, C., Wang, X., 2020a. Cooling control effect of water mist on thermal runaway propagation in lithium ion battery modules. Appl. Energy 267, 115087. https://doi.org/10.1016/j.apenergy.2020.115087.
Liu, Y., Duan, Q., Xu, J., Li, H., Sun, J., Wang, Q., 2020b. Experimental study on a novel safety strategy of lithium-ion battery integrating fire suppression and rapid cooling. J. Energy Storage 28, 101185. https://doi.org/10.1016/j.est.2019.101185.
Liu, T., Hu, J., Tang, Q., Zhu, X., Wang, X., 2021a. Mitigating overcharge induced thermal runaway of large format lithium ion battery with water mist. Appl. Therm. Eng. 197, 117402 https://doi.org/10.1016/j.applthermaleng.2021.117402.
Liu, T., Hu, J., Tao, C., Zhu, X., Wang, X., 2021b. Effect of parallel connection on 18650-type lithium ion battery thermal runaway propagation and active cooling prevention with water mist. Appl. Therm. Eng. 184, 116291 https://doi.org/10.1016/j.applthermaleng.2020.116291.
Liu, Y., Yang, K., Zhang, M., Li, S., Gao, F., Duan, Q., Sun, J., Wang, Q., 2022. The efficiency and toxicity of dodecafluoro-2-methylpentan-3-one in suppressing lithium-ion battery fire. J. Energy Chem. 65, 532–540. https://doi.org/10.1016/j.jechem.2021.05.043.
Matheson, I.B.C., King, A.D., 1978. Solubility of gases in micellar solutions. J. Colloid Interface Sci. 66, 464–469. https://doi.org/10.1016/0021-9797(78)90066-8.
Meng, X., Yang, K., Zhang, M., Gao, F., Liu, Y., Duan, Q., Wang, Q., 2020. Experimental study on combustion behavior and fire extinguishing of lithium iron phosphate battery. J. Energy Storage 30, 101532. https://doi.org/10.1016/j.est.2020.101532.
Meng, X., Li, S., Fu, W., Chen, Y., Duan, Q., Wang, Q., 2022. Experimental study of intermittent spray cooling on suppression for lithium iron phosphate battery fires. eTransportation 11, 100142. https://doi.org/10.1016/j.etran.2021.100142.
Russo, P., Di Bari, C., Mazzaro, M., De Rosa, A., Morriello, I., 2018. Effective fire extinguishing systems for lithium-ion battery. Chem. Eng. Trans. 67, 727–732. https://doi.org/10.3303/CET1867122.
Said, A.O., Stoliarov, S.I., 2021. Analysis of effectiveness of suppression of lithium ion battery fires with a clean agent. Fire Saf. J. 121, 103296 https://doi.org/10.1016/j.firesaf.2021.103296.
Said, A.O., Garber, A., Peng, Y., Stoliarov, S.I., 2021. Experimental Investigation of Suppression of 18650 Lithium Ion Cell Array Fires with Water Mist. Fire Technol. https://doi.org/10.1007/s10694-021-01151-9.
Tao, C., Ye, Q., Wang, Chunmei, Qian, Y., Wang, Chenfang, Zhou, T., Tang, Z., 2020. An experimental investigation on the burning behaviors of lithium ion batteries after different immersion times. J. Clean. Prod. 242, 118539 https://doi.org/10.1016/j.jclepro.2019.118539.
Un, C., Aydın, K., 2021. Thermal runaway and fire suppression applications for different types of lithium ion batteries. Vehicles 3, 480–497. https://doi.org/10.3390/vehicles3030029.
Wang, H., Tang, A., Wang, K., 2011. Thermal behavior investigation of LiNi1/3Co1/3Mn 1/3O2-based li-ion battery under overcharged test. Chin. J. Chem. 29, 27–32. https://doi.org/10.1002/cjoc.201190056.
Wang, Q., Shao, G., Duan, Q., Chen, M., Li, Y., Wu, K., Liu, B., Peng, P., Sun, J., 2016. The efficiency of heptafluoropropane fire extinguishing agent on suppressing the lithium titanate battery fire. Fire Technol. 52, 387–396. https://doi.org/10.1007/s10694-015-0531-9.
Wang, Q., Li, K., Wang, Y., Chen, H., Duan, Q., Sun, J., 2018. The efficiency of dodecafluoro-2-methylpentan-3-one on suppressing the lithium ion battery fire. J. Electrochem. Energy Convers. Storage 15, 1–10. https://doi.org/10.1115/1.4039418.
Wang, Q., Mao, B., Stoliarov, S.I., Sun, J., 2019. A review of lithium ion battery failure mechanisms and fire prevention strategies. Prog. Energy Combust. Sci. 73, 95–131. https://doi.org/10.1016/j.pecs.2019.03.002.
Weng, J., Ouyang, D., Yang, X., Chen, M., Zhang, G., Wang, J., 2019. Alleviation of thermal runaway propagation in thermal management modules using aerogel felt coupled with flame-retarded phase change material. Energy Convers. Manag. 200, 112071 https://doi.org/10.1016/j.enconman.2019.112071.
Wilke, S., Schweitzer, B., Khateeb, S., Al-Hallaj, S., 2017. Preventing thermal runaway propagation in lithium ion battery packs using a phase change composite material: an experimental study. J. Power Sources 340, 51–59. https://doi.org/10.1016/j.jpowsour.2016.11.018.
Xu, J., Guo, P., Duan, Q., Yu, X., Zhang, L., Liu, Y., Wang, Q., 2020. Experimental study of the effectiveness of three kinds of extinguishing agents on suppressing lithium-ion battery fires. Appl. Therm. Eng. 171 https://doi.org/10.1016/j.applthermaleng.2020.115076.
Xu, J., Duan, Q., Zhang, L., Liu, Y., Zhao, C., Wang, Q., 2022. Experimental study of the cooling effect of water mist on 18650 lithium-ion battery at different initial temperatures. Process Saf. Environ. Protect. 157, 156–166. https://doi.org/10.1016/j.psep.2021.10.034.
Yuan, S., Chang, C., Yan, S., Zhou, P., Qian, X., Yuan, M., Liu, K., 2021. A review of fire-extinguishing agent on suppressing lithium-ion batteries fire. J. Energy Chem. 62, 262–280. https://doi.org/10.1016/j.jechem.2021.03.031.
Zhang, L., Duan, Q., Liu, Y., Xu, J., Sun, J., Xiao, H., 2020a. Experimental investigation of water spray on suppressing lithium-ion battery fires. Fire Saf. J. 103117 https://doi.org/10.1016/j.firesaf.2020.103117.
Zhang, L., Li, Y., Duan, Q., Chen, M., Xu, J., Zhao, C., Sun, J., Wang, Q., 2020b. Experimental study on the synergistic effect of gas extinguishing agents and water mist on suppressing lithium-ion battery fires. J. Energy Storage 32, 101801. https://doi.org/10.1016/j.est.2020.101801.
Zhang, L., Li, Y., Duan, Q., Chen, M., Xu, J., Zhao, C., Sun, J., Wang, Q., 2020c. Experimental study on the synergistic effect of gas extinguishing agents and water mist on suppressing lithium-ion battery fires. J. Energy Storage 32. https://doi.org/10.1016/j.est.2020.101801.
Zhang, L., Duan, Q., Meng, X., Jin, K., Xu, J., Sun, J., Wang, Q., 2022. Experimental investigation on intermittent spray cooling and toxic hazards of lithium-ion battery thermal runaway. Energy Convers. Manag. 252, 115091 https://doi.org/10.1016/j.enconman.2021.115091.
Zhao, J., Xue, F., Fu, Y., Cheng, Y., Yang, H., Lu, S., 2021. A comparative study on the thermal runaway inhibition of 18650 lithium-ion batteries by different fire extinguishing agents. iScience 24, 102854. https://doi.org/10.1016/j.isci.2021.102854.
Zhuang, W., Zhu, S., Li, X., Hao, X., 2019. Experimental study on suppression of fire and explosion of lithium iron phosphate battery by inert gas. In: Proc. 2018 IEEE Int. Conf. Saf. Prod. Informatiz. IICSPI, pp. 2018 57–61. https://doi.org/10.1109/IICSPI.2018.8690468.